Received 16 June 2025, accepted 7 July 2025, date of publication 15 July 2025, date of current version 29 July 2025.
Digital Object Identifier 10.1109/ACCESS.2025.3589492

RESEARCH ARTICLE

Fast Field Strength Prediction Using Modern Machine Learning in European Cities From Few RF-EMF Measurements: A Neural Tangent Kernel Perspective

MOHAMMED MALLIK[1], (Member, IEEE), JORN SCHAMPHELEER[2], LAURENT CLAVIER[3], (Senior Member, IEEE), AND MARGOT DERUYCK[2], (Member, IEEE)
[1]Univ Lyon, INSA Lyon, CITI, F-69621 Villeurbanne, France
[2]Department of Information Technology, IMEC, Ghent University, 9000 Ghent, Belgium
[3]IMT Nord Europe, 59650 Lille, France

Corresponding author: Mohammed Mallik (mohammed.mallik@insa-lyon.fr)

ABSTRACT The rapid growth of 5G and 6G networks, with their dense deployments, millimeter-wave communications, and dynamic beamforming, necessitates scalable simulation tools for performance evaluation, network design, and electromagnetic field (EMF) exposure assessment. EMF simulations model exposure across frequency, space, and time, typically based on base stations, user devices, and deterministic and empirical models. These simulations are essential for network operators and researchers for network planning, assessing human exposure to RF-EMF, and ensuring compliance with safety regulations considering factors like frequency, power levels, antenna configurations, and the environment, but they often require extensive computational resources and large simulation time. To address this, we propose an infinitely wide convolutional neural network approach for fast and accurate EMF exposure estimation. Remarkably, taking the width of a neural network to infinity allows for improved computational performance. We compute a convolutional neural tangent kernel from the infinite-width network to perform matrix imputation for exposure estimation. Proposed method estimates exposure fields using less than 7% of simulation points and outperforms other machine learning models, predicting exposure levels which fall below the safety limit set by ICNIRP in under $\mathbf{3,66 \times 10^{-3}}$ seconds.

INDEX TERMS EMF exposure, kernel regression, infinite width convolutional neural network, neural tangent kernel, semi-supervised learning.

I. INTRODUCTION

Wireless communication technologies have become an essential part of our everyday lives, integrating in with the surroundings with ease. Thus, it is crucial to keep updated on phenomena related to wireless systems, like exposure to radio-frequency electromagnetic fields (RF-EMFs). Numerous sources of electromagnetic fields (EMFs), including WiFi, 2G, 3G, 4G, and the newest 5G mobile technologies, contribute to the electromagnetic medium in an urban setting.

The associate editor coordinating the review of this manuscript and approving it for publication was Su Yan.

Although 5G promises significant advancements over previous generations [1], [2], [3], many 6G research topics necessitate the use of ray tracing (RT) to simulate particular radio environments in order to assess a network's performance. Examples include radio-based localization [4], multi-modal sensing [5], integrated sensing and communications (ISAC) [6], and the majority of the use-cases of the recently introduced machine learning (ML)-based transceiver algorithms [7].

This makes simulation a major player in planning and designing 4G, 5G, and 6G networks with respect to optimal coverage, capacity, and performance under EMF constraints. The regulatory organizations like the International

Commission on Non-Ionizing Radiation Protection (ICNIRP), the Institute of Electrical and Electronics Engineers (IEEE), and the World Health Organization, (WHO), conducted extensive amounts of work on Research into the determination of exposure guidelines for EMF on humans. This is imperative because base stations and mobile devices that generate EMFs in radio communication need to be within legal limits on exposure levels [8], [9], [10]. This calls for the replication of exposure effects due to wireless technologies. In real-life complex scenarios with frequency bands, antenna configurations, power levels, propagation models, user density, it requires simulation of behaviors and mobility; the urban environment includes challenging signal obstruction, multipath effects, and beamforming optimization. Advanced simulations can provide accurate network performance assessment and the verification of compliance with EMF exposure regulations with low computational costs. Reducing simulation time is critical, as traditional methods often require hours or days, prompting the development of faster, AI-driven solutions.

There are two major approaches in the literature, namely simulation and stochastic geometry, that are applied to map a cellular network topology to its performance.

A. DETERMINISTIC AND EMPIRICAL PROPAGATION MODELS

In a simulation based setup, the precise configuration of a network (antenna location, height, azimuth, etc.) are fed into a simulator along with a statistical model of the channel gains. The simulator then calculates the Signal-to-Interference-plus-noise ratio (SINR) at each possible user location for a given realization of the BS-to-user channels and calculates different performance metrics such as coverage, exposure etc. Accurately assessing exposure in a specific metropolitan area is very difficult. Ray Tracing (RT) techniques, which model the propagating field using an array of rays that go through the environment and reflect, diffract, and scatter, are the foundation of deterministic propagation tools like Veneris-Opal [11] and Atoll [12]. These methods make use of the optical ray, a high-frequency approximation of the Maxwell equations. However, it is nearly impossible to evaluate all active networks and devices in order to determine the EMF levels. There are surprisingly few open source tools and libraries accessible, even though RT approaches are used in a large number of works and new ways are being introduced on a regular basis [13]. The majority of research software is either solely commercially licensed or not distributed. SPLAT! (https://www.qsl.net/kd2bd/splat.html) and Radio Mobile (http://www.ve2dbe.com/), which are radio frequency signal propagation simulators that account for terrain losses, are two examples of open source simulators that do not require RT. The computing engine used by many of the open source programs is Matlab [14], which needs a license. For example, SimRIS [15] supports customizable intelligent surfaces, and NYUSIM [16] offers bespoke channel models for 5G and 6G simulation. Among the proprietary commercial tools that include at least a similar set of features, including moving elements and antenna radiation patterns, we can only find Altair Feko (https://www.altair.com/feko-applications/) or Siradel solutions (https://www.siradel.com/solutions/software/). One of the major pitfall is all these software's requires significant resource and time to simulate difference metric in a given area. For example in [17], to simulate exposure in a 1 km^2 area in Lille, France with only 1 BS, approximately 30 minutes to generate 1 realization of the network.

B. RANDOM SPATIAL PATTERNS

An alternative to simulation that assesses network performance analytically is stochastic geometry (SG). Localization, car radar [18], and cumulated interference power [19] are only a few of the many applications for it. To determine the mean or Cumulative Distribution Function (CDF) of performance indicators (such as coverage, EMF exposure, etc.), stochastic geometry is a helpful tool [20]. However, neither the precise site to be investigated nor the user's geographical location have a direct relationship to this estimated information. Motivated by tractability, SG-based analytical expressions can be found in the literatures [21], [22], [23], and [24]. In order to guarantee tractability, these expressions rely on a number of frequently unreasonable simplifying assumptions about the wireless network. A key principle of SG-based models is that it is possible to characterize the positions of users and BSs in a network as realizations of stationary two-dimensional (2D) random point processes. For instance, two limitations of SG is given below:

1) NON-HOMOGENEOUS DISTRIBUTION

The majority of research based on stochastic geometry uses a homogeneous Poisson point process (HPPP) to describe the base station placements. Although this streamlines the study, it fails to reflect the repulsive spatial structure seen in actual cellular networks; a Matern hard-core point process (HCPP) is a better model for base station locations, according to multiple studies [24]. However, the tractability of the analytical investigation of network performance is compromised by this more realistic modeling [25].

2) CORRELATED SHADOWING

Many stochastic geometry-based studies simplify channel modeling by either disregarding shadowing effects or treating shadowing as a spatially independent log-normal process. However, incorporating spatially correlated shadowing generally renders analytical derivations intractable using traditional stochastic geometry tools. Some works, such as [26], address correlated shadowing but adopt a specific shadowing model while omitting the path loss component to maintain mathematical feasibility. Another strategy found in the literature approximates interference—comprised of numerous log-normal shadowing terms—using a gamma distribution, significantly simplifying coverage probability analysis in [27].

Despite advances in this field, the wide variety of parameters, e.g., materials, sensor arrangement, or environment topology, make monitoring of EMF exposure relatively complex and often require a large number of measurements, which is both time-consuming and expensive. Moreover, these simulations are complex tasks because they involve taking into account a large number of base stations, different technologies and operators, and network configurations that are unknown to us, such as the powers and beams used by the base stations.

C. OUR STRATEGY

The main direction in the above discussion is that while simulations effectively address the needs of network configuration, they are limited by extensive computational time and resources. Conversely, SG-based models offer faster computations but lack the ability to provide location-specific insights of network performances. In this work, we take the middle path and propose a deep learning approach, delivering location-specific performance metrics which is exceptionally fast, accurate and computationally efficient. Essentially, our goal is to mimic the core functionality of a simulator in a time-efficient manner. At its core, a simulator performs a functional mapping, taking a network configuration as input and generating outputs such as location-dependent metrics - coverage, received signal strength, and EMF exposure. In this article, we propose an infinite width convolutional neural network to approximate this mapping, which does not require a large training set, thus overcoming the extensive time of simulators and training deep learning models.

This work aims to reconstruct the RF-EMF exposure across 3 major cities in Europe: Eindhoven, Utrecht and Zurich. The goal is to achieve fast and accurate exposure mapping for the entire area while minimizing the number of measurements required.

Based on a sparsely distributed location specific EMF exposure in the target area, To estimate the exposure maps, the proposed contribution is to train an infinite Convolutional Neural Network (CNN) for matrix imputation [28], [29]. In the infinite width limit [30], [31], [32], [33], artificial neural networks are analogous to kernel methods as they are related to Gaussian processes. This idea is expanded upon in the proposed approach (FAST-EMF), which uses a Convolutional Neural Tangent Kernel (CNTK) to fill in the sparse exposure maps [34]. Learning-based models (cGAN, ANN) are taken into consideration in order to assess and verify the performance of the suggested model. Despite relying on a few measurements, the developed method performs well in terms of computation time and accuracy of estimation.

The following is a summary of this paper's primary contributions:

- We present a unique method, FAST-EMF, that accurately and rapidly estimates an exposure field by taking into account neural networks' width limit. To ensure the consistency of the estimation, the network is infused with terrain knowledge.
- We assess the performance of the proposed approach for reconstructing the exposure field in an urban environment using a limited number of data points. The learning model's capacity to achieve this task quickly is demonstrated by a complementary analysis on its inference time.

The paper is structured as follows: Section I-D provides an explanation the background the estimation method. The suggested FAST-EMF method for estimating the exposure field in an urban setting is described in Section II. The performance of the suggested technique is evaluated both qualitatively and quantitatively in Section III. Sections IV and V provide the discussion and conclusion.

D. ESTIMATION METHOD

Matrix imputation is a technique for recovering missing values in an incomplete dataset and often uses learning-based approaches relying on statistical information from the whole dataset. Authors of [34] and [35] introduced an innovative approach for regression, and shape completion using incomplete data. Radhakrishnan et al. in [36], showed drug response prediction and authors of [34] showed classification by infinite neural networks. A very interesting direction was taken by the authors of [35], who addressed unsupervised 3D shape completion and reconstruction given incomplete scanned data. The authors propose a deep prior that was developed from the Neural Tangent Kernel (NTK). It is demonstrated that CNN-based shape patch completion has a striking resemblance to existing patches within the kernel feature space defined by the NTK due to the locality of these features. The work by Arora et al. [34] demonstrated that a fully-trained, sufficiently wide neural network is equivalent to a kernel regression predictor defined by the NTK. In this work, we propose to address the exposure map estimation problem as unobserved data imputation in matrices using infinitely wide CNN for CNTK [34]. The exposure map is reconstructed from a few exposures at sparse locations in target areas. A high-level overview of the proposed approach is depicted in Figure 1.

Our goal is to investigate a neural network-based method that is infinitely wide and does not require training on large data sets (full reference maps). The recently proposed Neural Tangent Kernel (NTK) [34] technique can be used to achieve this goal.

II. METHODOLOGY

A. INVERSE PROBLEM FORMULATION

This study focuses on estimating RF-EMF exposure maps across three major cities: Eindhoven, Utrecht, and Zurich, identified as the regions of interest (RoIs). Each RoI is represented as a rectangular grid of size $I \times J$, where sparse measurement points, randomly positioned within the area, serve as the basis for estimation. At each grid location (i, j), with $i \in \{1, \ldots, I\}$ and $j \in \{1, \ldots, J\}$, the EMF exposure

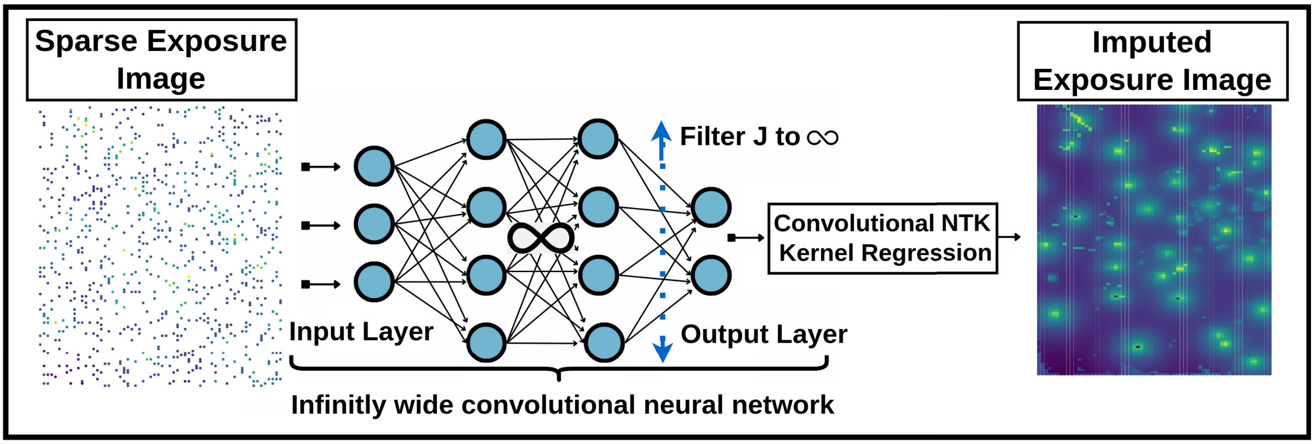

FIGURE 1. RF-EMF estimation by modern machine learning. The main contribution lies in constructing the kernel and designing the priors.

level $e_{(i,j)} \in \mathbb{R}^S$ is measured, with S representing the number of available measurements. The estimation task, framed as an inverse problem, involves reconstructing the exposure map $e \in \mathbb{R}^{I\times J}$ for the entire grid. The goal is to identify a predictive function $f_\theta : \mathbb{R}^S \to \mathbb{R}^{I\times J}$ that estimates exposure levels at unmeasured locations, with θ denoting the function's parameters. Techniques like kriging and statistical learning methods can be used to derive f_θ.

B. EMF EXPOSURE BY MODERN MACHINE LEARNING

An ANN was used in [37] to estimate exposure in a Paris urban area from a few sparsely distributed sensors. Using five input features, including position, transmitter distance to sensors, etc., as X and target exposure as labels Y, the ANN model was trained in that work by minimizing mean squared error (MSE) loss. The neural network used is a function γ_ψ given by:

$$\gamma_\psi(x) = \gamma_{\psi_k}\phi(\gamma_{\psi_{k-1}}\phi(\gamma_{\psi_{k-2}}\phi(\ldots(\gamma_{\psi_1}(x))\ldots)), \quad (1)$$

where x is the input and $\gamma_\psi \in \{1, \cdots, k\}$, are the layer functions. Usually, layer functions develop by joining basic scalar-valued functions termed neurons, which represent a linear function followed by a non-linear function as activation ϕ. The neural network's parameters are stored in the vector ψ_k and it is updated by the training process. As proven in work by Jacot et al. [38], for the over-parameterized or infinitely wide neural networks, they can be represented as a kernel function, which is similar to solving kernel regression, [34], [38]. The NTK is defined:

Definition (Neural Tangent Kernel): Let $f(w) : \mathbb{R}^P \to \mathbb{R}$ denote a neural network with initial parameters $w^{(0)}$. The ***neural tangent kernel,*** *$K : \mathbb{R} \times \mathbb{R} \to \mathbb{R}$ is a positive semi-definite function given by:*

$$K(x, x') = \langle \nabla f_x(w^{(0)}), \nabla f_{x'}(w^{(0)}) \rangle, \quad (2)$$

where $w^{(0)} \in \mathbb{R}^P$ denotes the parameters at initialization.

Reconstructing exposure maps with Convolutional NTK (CNTK) involves mapping the element coordinates in matrix γ to the observed entries in γ. A convolutional network with varying layers, kernel size, and convolution combined with downsampling is used to build the CNTK [34]. The following provides the connection between the CNN model and the CNTK:

$$K(x, x') = \langle \frac{\delta f(\theta, x)}{\delta W_{i,j,k,l}} \times \frac{\delta f(\theta, x')}{\delta W_{i,j,k,l}} \rangle, \quad (3)$$

where x and x' are input samples, θ represents parameters of the network, $w_{i,j,k,l}$ denotes the summation over the indices of the convolutional filters and their corresponding weights W, and the L-th layer CNTK kernel is given by:

$$K(x, x') = [\Theta^L(A, A')]_{i,j,i',j'} \quad (4)$$

A is a matrix, it is defined as $A \in \mathbb{R}^{C\times M\times N}$, where C is the number of channels. In unsupervised neural networks, previous studies have demonstrated that using priors [39], [40] which are drawn from a stationary distribution can perform well [41], [42] for inpainting tasks. In this work, A is initialized by a prior. The accuracy of the reconstruction is dependent on this prior that captures the relationship among the coordinates within the target matrix, resembling semi-supervised learning and such priors are widely used in tasks related to image processing [43]. Kernel regression with CNTK details are given in A.

C. PRIORS

In Bayesian learning, *priors* represent the initial beliefs or assumptions that are expressed as probability distributions or uncertainties, we have about the parameters. In the context of exposure estimation and infinite width limit neural networks, the prior A is independent of the observed exposure in the target matrix. In this work, minimizing the loss function maps elements of A to the coordinates of target γ_ψ. We experimented on 2 priors to initialize A: a Local Image Prior (LIP) [39], where A contains the measurement data randomly sampled from the RoIs, or a random i.i.d. tensor, where the channels are taken from a normal distribution (random normal prior - RNP). Recent studies have demonstrated that as the width of neural networks approaches infinity, their training behavior aligns closely with kernel regression using the Neural Tangent Kernel (NTK) [34], [38]. In this regime, training a network of infinite width becomes equivalent to solving a linear system, as the NTK for fully connected architectures can be efficiently computed in closed form [34], [38].

With only a fraction of a matrix's coordinates observed, the objective is to impute the unseen entries in $\gamma \in \mathbb{R}^{I \times J}$.

D. MODEL ARCHITECTURE

When the network width tends to infinity, the CNTK is derived using a CNN. The proposed CNN model is modified from [44] and has six convolutional layers, each using a kernel size of (3, 3) and zero padding to preserve spatial dimensions, followed by *LeakyReLU* activation, where 0.05 and 1 are the slopes, providing nonlinearity while maintaining kernel tractability. Transposed convolution, upsampling, or trilinear upsampling are employed to change the spatial dimensions of the feature maps. Training methods, activation functions, layers, and model parameters are based on [45] and [46], and a stabilization technique is applied to mitigate exploding or vanishing gradient issues during training.

The matrix's dimensions can be 128 × 128, 64 × 64, or 32 × 32. The grid's dimensions in this work were restricted to 32 × 32.

E. EXPOSURE ESTIMATION - CNTK

In this work, CNTK uses image coordinate features as semi-supervised learning. This is equivalent to mapping from coordinate features to observed entries in the target matrix $\hat{\gamma}$ as a linear combination of the unobserved entries in the target matrix γ to calculate the coefficients ω of the kernel model. if the measured exposure value at the observed coordinates is vector y, then ω is given by solving linear systems:

$$\omega = \psi^{-1}.y, \tag{5}$$

For a missing entry at (i, j) coordinate in $\hat{\gamma}$, kernel regression with CNTK matrix K, based on the observed entries using a weighted sum of nearby values. Details are given in Appendix Sec. B.

III. RESULTS

A. EVALUATION METRICS

To evaluate the performance of our system, we use two different metrics. The error $\left|y - \hat{y}\right|$ between the predicted value $\hat{y}$ and the reference value y is initially utilized.

To have a summarized metric we will consider the root mean squared error (RMSE), mean absolute error (MAE) [47] given by:

$$RMSE = \sqrt{\frac{1}{n}\sum_{i=1}^{n}\left(Y_i - \hat{Y}_i\right)^2}. \tag{6}$$

$$MAE = \frac{1}{n}\sum_{i=1}^{n}\left(\Upsilon_i - \Upsilon'_i\right) \tag{7}$$

B. IMPLEMENTATION DETAILS AND DATASETS

The regions of interest (RoIs) selected for this study represent the largest possible rectangular areas in Eindhoven, Utrecht, and Zurich can be seen in Fig. 2. Specifically, these RoIs cover areas of 36 km^2, 36 km^2, and 22 km^2, respectively. Given the considerable size of these RoIs, we adopted a strategy of subdividing them into smaller grids for the imputation process. For instance, within Eindhoven, we first selected a rectangular area of 36 km^2 and subsequently divided it into eight smaller sub-grids, each with grid resolution of 32 × 32, which together cover a total area of 36 km^2. After the matrix imputation process, each matrix was stitched together to form the entire RoI. The dataset for the proposed method consisted of a minimum number of points selected from three regions of interest (RoIs), starting with 2% of the total points (Eindhoven: 168, Utrecht: 189, Zurich: 252) and increasing to 6% (Eindhoven: 488, Utrecht: 544, Zurich: 680) to reconstruct exposure at all regions. The dataset consists of matrices, where each matrix is $\gamma \in \mathbb{R}^{M \times N}$, where M and N are the number of rows and columns of the map grid.

For the simulations the GRAND (Green Radio Access Network Design) network planner developed by WAVES research group at Ghent University has been used [48], [49], which is based on the algorithm proposed in [50]. GRAND develops wireless access networks for various technologies while optimizing the network towards various KPI (Key Performance Indicators) such as coverage, power consumption and human exposure in both uplink and downlink. The planner is capacity-based meaning that it develops the network based on the instantaneous bit rate request by the users active in the considered environment. As input, it uses a 3D map of the environment to properly determine the propagation from the base stations, the possible base station locations in that environment as well as the location and the bit rate request from the users. To design the network, the GRAND tool uses a heuristic algorithm, in particular a MILP (Mixed Integer Linear Programming) solving algorithm, creating a graph network of the possible solutions. The GRAND tool decides where to place the base station locations as well as their settings (such as e.g., the input power of the antennas). As output, the planner delivers various quantitative metrics such as the overall network exposure, the exposure in each grid point, user coverage, geometrical coverage, the base stations' and the network's power consumption, etc. The dataset for selected RoIs (Utrecht, Zurich and Eindhoven) were generated in a grid with 32152, 38974, 35564 points which served as the groundtruth for the 3 RoIs.

C. GENERATIVE MODEL AND ARTIFICIAL NEURAL NETWORK

The proposed FAST-EMF is compared with Generative Adversarial Network (cGAN) [51] and Artificial Neural Network (ANN) as proposed in [37] in a regression setting. These deep learning models are pre-trained on the same

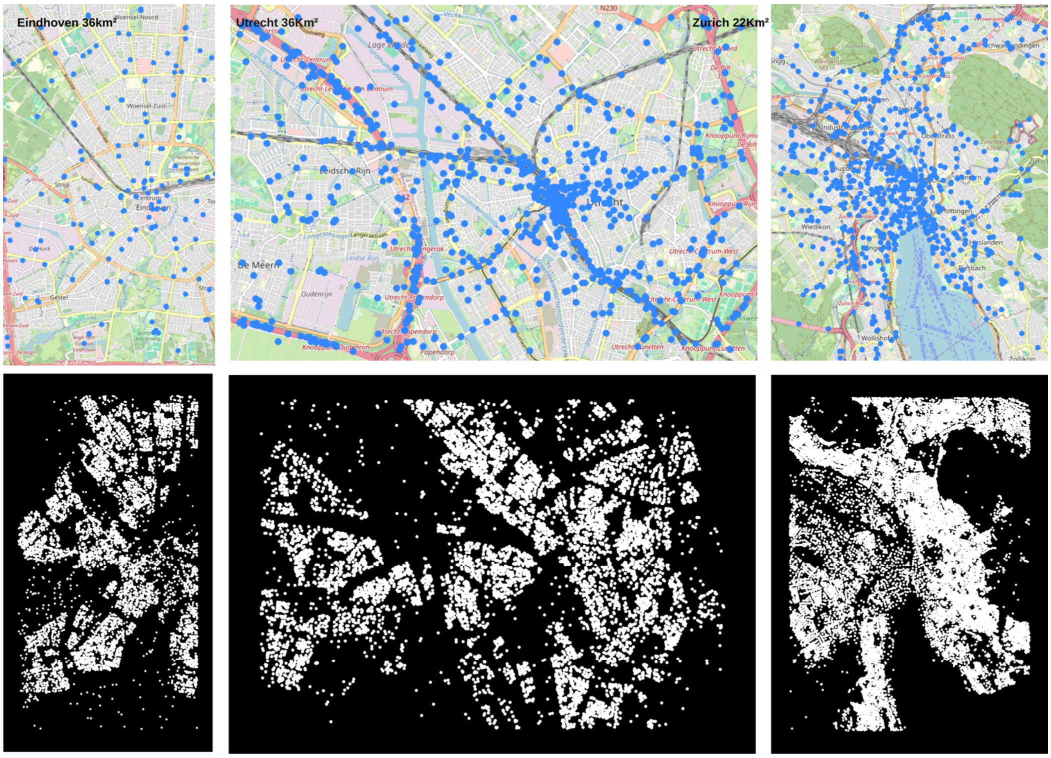

FIGURE 2. The region of interest. a) shows the experimental 1km^2 area, blue represents transmitters, and b) reveals the city topology (buildings) extracted as raster from OpenStreetMap.

dataset as FAST-EMF. The dataset was divided into train and test and validation, where the train data was the same dataset that gave the best result for FAST-EMF, i.e for Eindhoven, Utrecht, and Zurich 6% of the measurement. Details are given in Appendix Sec. D, C.

D. VISUAL ANALYSIS

1) FAST-EMF

Figure 3 shows the effectiveness of the proposed approach in 3 target RoIs compared with the reference maps generated by the GRAND simulator. The estimated exposure map was reconstructed by 2%, 4%, and 6% of all measurements as observed exposure for imputation. We only visualize the best estimation, which was obtained using 6% of the location points of each RoI as input.

In Figure 3, specifically in the third row (error maps), the estimation errors for all methods remain relatively small, ranging from -7.5 dB to -15 dB. However, in the second row, which depicts the reconstruction of the Utrecht area, noticeable irregularities appear along the edges of the stitched matrices, particularly in the upper and lower middle sections. These inconsistencies arise because the Utrecht exposure exhibits significant variations that were not adequately captured by the method. In contrast, no such artifacts are observed in the reconstructed areas for Eindhoven and Zurich.

2) cGAN, ANN

In these regions, both the cGAN and ANN models struggle to generalize EMF exposure effectively. This limitation can be attributed to the small training dataset, representing only 6% of the total data across the three RoIs near the prediction points. Specifically, the training datasets consisted of 488, 544, and 680 samples for Eindhoven, Utrecht, and Zurich, samples that were sufficient for FAST-EMF but remained insufficient for training a robust generative model or an ANN. As shown in Fig. 4, the models fail to capture the spatial structure accurately. Expanding the training set or using advanced transfer learning techniques could potentially address these limitations and improve model performance.

E. COMPARATIVE ANALYSIS OF STATISTICAL RESULT

1) IMPACT OF OBSERVED POINTS DENSITY

Table 1 summarizes the evaluation of the proposed method using various models and priors to assess the accuracy of the CNTK approach. In the 36 km^2 Eindhoven area, observed exposure data was sampled at different densities: 2% (168 samples, 5 measurements/km^2), 4% (328 samples, 10 measurements/km^2), and 6% (488 samples, 13 measurements/km^2). These samples were used to impute the region of interest (RoI) and to train the generative model and ANN. The cGAN and ANN models have high RMSE values of $1{,}813.10^{-1}$ V/m and $1{,}014.10^{-1}$ V/m, respectively, indicating poor performance in estimating exposure in the test regions, as shown in Fig. 4. In contrast, remarkably, increasing the number of observed locations led to a steady decrease in RMSE and MAE for the CNTK method, reaching values as low as $1{,}007.10^{-1}$ V/m and $2{,}510.10^{-2}$ V/m for LIP, respectively.

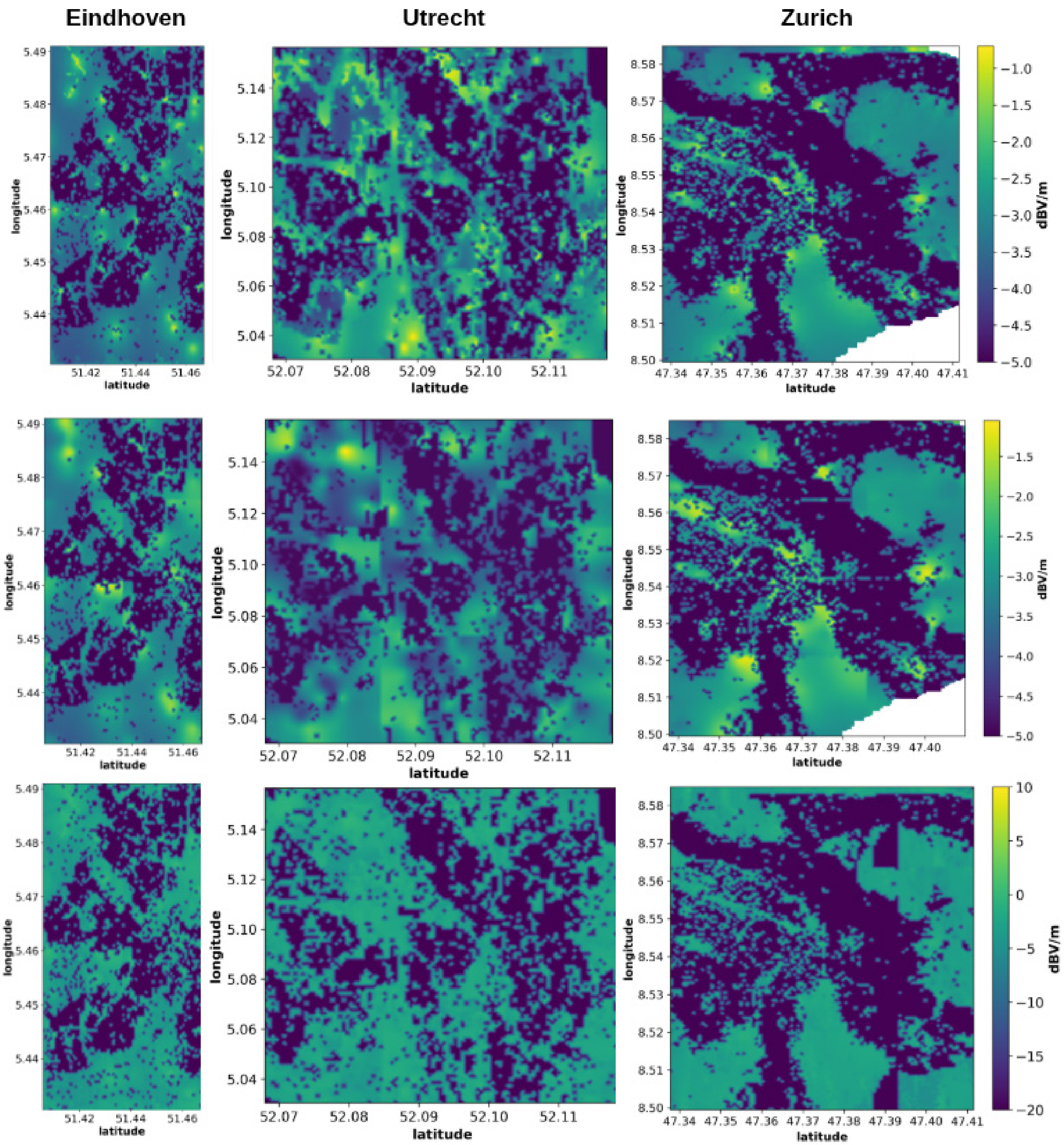

FIGURE 3. Comparison of inferred exposure maps of the proposed method in Eindhoven, Utrecht, and Zurich. 1st row: (left to right): The ground truth maps from the simulator. 2nd row: (left to right): The imputed maps and 3rd row (left to right): the error map of the RoIs. Estimated maps are visualized for 6% of the exposure points from the ground truth map, specifically 488, 544, and 680 measurements for Eindhoven, Utrecht, and Zurich respectively used as input for estimation.

In Utrecht and Zurich, a similar trend can be observed, where 6% of the exposure data (544 points, 16 locations/km^2), and 680 points (28 locations/km^2) respectively are utilized. The cGAN and ANN models exhibit relatively high RMSE and MAE values (2,65.10^{-2} V/m and 2,51.10^{-2} V/m, respectively). Although these values are similar, visual analysis shows that both models struggle to accurately estimate and generalize exposure levels in the RoIs. On the other hand, the CNTK method improves steadily with increased number of observed locations, reaching low RMSE of 2,41.10^{-2} V/m. This underlines the robustness of the CNTK while using minimum observed data effectively.

To validate the RMSE results, Fig. 5 highlights how CNTK effectively captures the behavior of the input variables across three RoIs. This demonstrates the model's ability to learn the underlying structure and characteristics of the exposure data.

TABLE 1. The comparison of reference and estimated EMF exposure levels is presented across three regions of interest (RoIs). For all methods, both RMSE and MAE metrics are evaluated. Specifically, the estimation errors for the CNTK approach using three priors—LIP and RNP are detailed. Furthermore, the analysis includes a breakdown of the computational time and resources required for each method.

	METHOD	POINTS	RMSE$_{LIP}$	RMSE$_{RNP}$	MAE$_{LIP}$	MAE$_{RNP}$	TIME$_{approx.}$	RESOURCE
Eindhoven	CNTK	2% 168	$1,41.10^{-1}$	$1,50.10^{-1}$	$4,3.10^{-2}$	$4,40.10^{-2}$	-	
		4%, 328	$1,20.10^{-1}$	$1,25.10^{-1}$	$2,90.10^{-2}$	$2,91.10^{-2}$	-	-
		6%, 488	$\mathbf{1,00.10^{-1}}$	$1,01.10^{-1}$	$2,51.10^{-2}$	$2,62.10^{-2}$	$\mathbf{8,43.10^{-4}}$ sec	**300MB**
	cGAN	6%, 488	$1,83.10^{-1}$	-	-	-	$\sim$ 23 min	10GB VRAM
	ANN	6%, 488	$1,01.10^{-1}$	-	-	-	15 sec	3GB VRAM
Utrecht	CNTK	2% 189	$2,52.10^{-2}$	$2,51.10^{-2}$	$1,21.10^{-2}$	$1,14.10^{-2}$	-	
		4%, 369	$2,42.10^{-2}$	$2,46.10^{-2}$	$1,11.10^{-2}$	$1,11.10^{-2}$	-	
		6%, 544	$\mathbf{2,40.10^{-2}}$	$2,41.10^{-2}$	$1,10.10^{-2}$	$1,10.10^{-2}$	$\mathbf{1,04.10^{-3}}$ sec	**300MB**
	cGAN	6%, 544	$2,70.10^{-2}$	-	-	-	$\sim$ 18 min	10GB VRAM
	ANN	6%, 544	$2,513.10^{-2}$	-	-	-	3.2 sec	3GB VRAM
Zurich	CNTK	2% 252	$1,27.10^{-2}$	$1,270.10^{-2}$	$5,53.10^{-3}$	$5,51.10^{-3}$	-	-
		4%, 492	$1,13.10^{-2}$	$1,13.10^{-2}$	$4,30.10^{-3}$	$4,32.10^{-3}$	-	
		6%, 680	$\mathbf{1,10.10^{-2}}$	$1,11.10^{-2}$	$4,10.10^{-3}$	$4,15.10^{-3}$	$\mathbf{1,02.10^{-3}}$ sec	**300MB**
	cGAN	6%, 680	$1,72.10^{-2}$	-	-	-	$\sim$ 24 min	10GB VRAM
	ANN	6%, 680	$2,81.10^{-2}$	-	-	-	3.2 sec	8GB VRAM

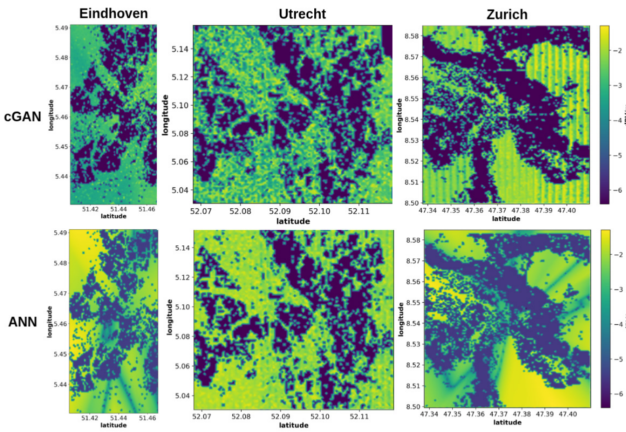

FIGURE 4. Estimated exposure map by cGAN and ANN. Poor generalization performance can be observed due to a lack of training samples.

As a result, the predictions closely align with the observed exposure and feature variables.

For a more detailed analysis, Fig. 6 presents a comparison between CNTK estimations and reference values using 100 samples. The figure clearly shows that the estimated kernel has successfully learned the features dynamics, enabling it to produce accurate predictions in comparing with the reference exposure data.

2) EFFECT OF PRIORS

We demonstrate that the accuracy of the proposed CNTK method can be influenced by the choice of *priors*. Specifically, we initialized the priors using two different approaches: local image points (LIP), and random normal distribution (RNP). The findings reveal that when the priors are initialized with LIP, the method achieves better performance compared to RNP. For instance, in Eindhoven, the LIP initialization yields an RMSE of $1,00.10^{-1}$ V/m, whereas RNP result in RMSE values of $1,01.10^{-1}$ V/m.

This trend continues in the other regions. For example, for Utrecht and Zurich, the RMSE of RNP initialization is $2,41.10^{-2}$ V/m and $1,11.10^{-2}$ V/m. However, LIP as the prior has a lower RMSE value of $2,41.10^{-2}$ V/m. In this case, the priors yielded better performance compared to each other. These results show the importance of selecting an appropriate prior in infinite-width networks and how this influences the performance of exposure estimation.

F. TIME EFFICIENCY AND RESOURCE

To find the efficiency of the proposed method, it was evaluated w.r.t. time and computational resources spent on training as well as inference. The performances, as listed in Table 2 of cGAN and ANN during testing had training times of about 23 minutes and 3.2 seconds on a system equipped with an Intel Core i7, NVIDIA RTX ADA 3500 GPU-16GB, and 32GB of memory. Also, the cGAN model trained on more than 500 epochs, while ANN finished training within 100 epochs. Memory Consumption: Both models were voracious, each required about 9GB RAM, 3 to 10 GB GPU memory for the three Regions of Interest.

In contrast, the proposed CNTK method significantly outperformed these approaches in terms of speed and resource efficiency. For training and imputing matrices over large areas, the CNTK required only $\mathbf{1.28} \times \mathbf{10^{-3}}$ seconds for a 36 km^2 area in Eindhoven, $\mathbf{3.66} \times \mathbf{10^{-3}}$ seconds for 36 km^{2}in Utrecht, and $\mathbf{1.65} \times \mathbf{10^{-3}}$ seconds for 24 km^2 in Zurich, as detailed in Table 1. Additionally, it achieved this using just 300MB of RAM. That means, this method can

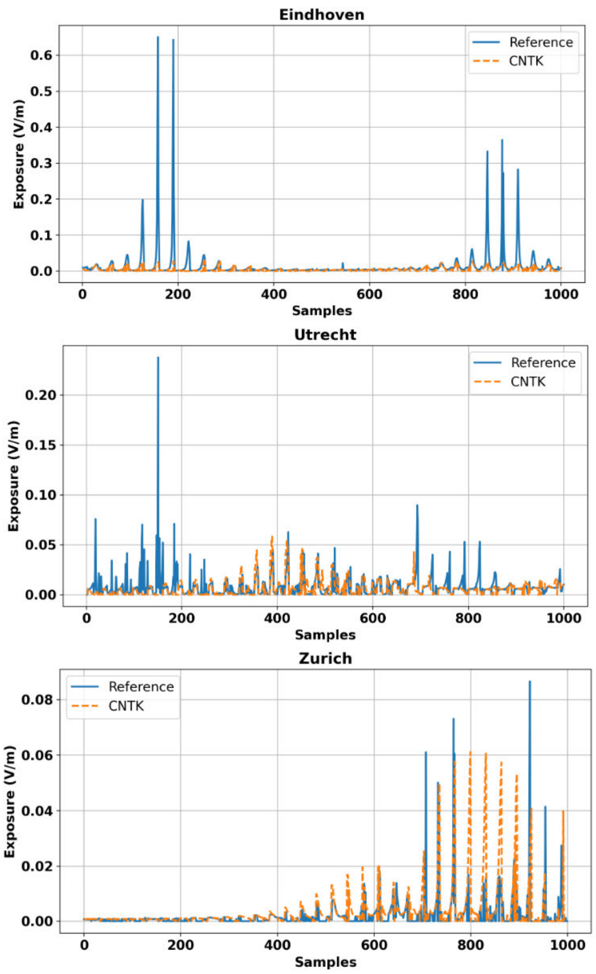

FIGURE 5. The plot shows the comparison of the reference and estimated EMF exposure levels for the first 1000 samples over 3 RoIs when LIP prior is used. For all 3 areas, CNTK estimates are closely aligned to the reference.

be used any modern laptop or PC without any use of large computational resource(for example: GPUs).

These results demonstrate the CNTK method's suitability for fast and accurate estimation of network performance metrics such as exposure, coverage, and received signal strength (RSS), all while demanding minimal computational resources.

IV. DISCUSSION

In this study, presents an infinite-width neural network-based approach, FAST-EMF, for estimating EMF exposure as a performance metric from minimum number of measurement points in 3 large cities in Europe. The study focused on minimizing the number of measurement points required to reconstruct exposure levels in three major European cities. Given that simulators and other techniques require significant computational resource and time, the objective was to develop a method capable of estimating exposure in realistic urban environments with minimal data. This approach not only reduces the burden of data collection but also

TABLE 2. Comparative analysis of time and computational resources required by the proposed method and other tools. Details of the RoIs are given in III-B. * The GRAND simulator reserves the memory for the solver component for its optimization techniques.

Method	Memory	Inference approx
FAST-EMF	**300 MB RAM**	$\mathbf{8,058.10^{-5}}$s per image
GRAND Simulator	10-15 GB RAM*	8 min/RoI
cGAN	10 GB VRAM	23 min/RoI
ANN	3 GB VRAM	3.2 seconds/RoI

ensures that assessments can be conducted efficiently without compromising accuracy. from the link between infinite width network and kernel methods, the study addressed the challenges of large-scale urban analysis in a resource efficient manner. The proposed method was evaluated and compared with deep learning techniques, cGAN and ANN across various parameters such as feature density, initialization of priors, computational time and resource efficiency.

The results showcase the superiority of the FAST-EMF approach over other deep learning approaches, cGAN and ANN. Even utilizing fewer measurements in the grid, CNTK method consistently outperforms other techniques. This observation underscores the effectiveness of the proposed methodology in accurately estimating EMF exposure with minimum number of locations which is achievable by time consuming learning based methods, a feature distinct from both other schemes.

One remarkable advantage of the CNTK approach is its adaptability across varying observed entries densities. The analyses revealed that the method maintains consistent performance even with limited locations, showcasing its robustness in real-world scenarios. Furthermore, the CNTK method demonstrated efficiency, requiring significantly less time ($\mathbf{3.660 \times 10^{-3}}$ s) and computational resources compared to cGAN and ANN, owing to the simple closed form formula of the tangent kernel [34], [38]. The main advantage of the proposed method is in solving kernel regression with CNTK as it involves solving linear systems of equations, which efficiently handles complex data patterns while optimizing computational resources.

Although CNTK produces satisfactory outcomes under many settings, low density measurement points show performance decrease. Furthermore, the proposed model can make use of a number of neural network design strategies, including batch normalization, skip connections, kernel initializers, etc, to increase the suggested method's estimation accuracy. When it comes to situations with a limited number of available measurements, the suggested technique performs better than cGAN and ANN. Additionally, the proposed method stands out for its speed and accuracy in estimating the exposure in large areas.

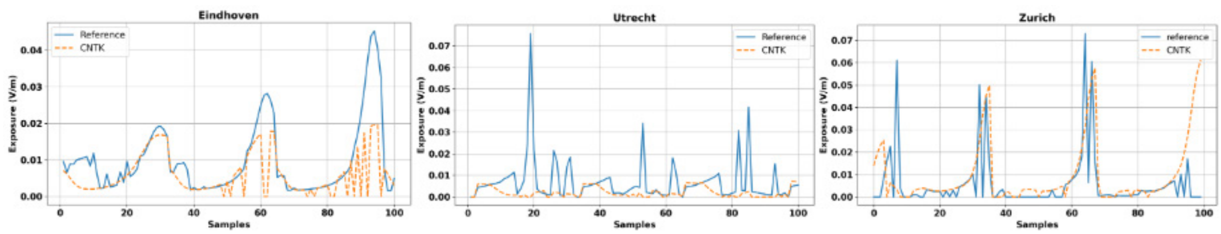

FIGURE 6. A more detailed closer look at the first 100 samples of the reference and estimated exposure by CNTK.

V. CONCLUSION

This study presents FAST-EMF, a innovative method based on infinite-width convolutional neural networks (CNNs) for estimating RF-RMF exposure in three major European cities: Eindhoven, Utrecht, and Zurich, using only a limited number of measurements. Unlike conventional deep learning approaches such as cGANs or ANNs, which require large training datasets and substantial training time due to their complex architectures and high parameter counts, our method significantly reduces both data and computational requirements. For 3 RoIs larger than 20 km^2, FAST-EMF can accurately estimate exposure using fewer than 7% of measurement points, with a computational time of less than 3.66×10^{-3} seconds. Rather than depending on oversimplified signal propagation models, FAST-EMF effectively captures complex propagation dynamics in urban environments, taking into account detailed building characteristics. In summary, the proposed method offers a balance between accuracy, computational efficiency, and adaptability, making it a promising solution for electromagnetic field (EMF) exposure estimation in large areas. Future work will focus on extending this framework to the temporal domain and integrating it with a physics based model using CNTK for dynamic exposure map forecasting.

APPENDIX

A. CNTK

We provide the CNTK formulation using the equation in (4) in the main text. The tensor $\Theta \in \mathbf{R}^{m\times n\times m\times n}$ was defined and was used in classification setting as [34]. In this case the CNTK is a 4-dimensional tensor.

Definition: Let γ_ψ represent a L layer convolutional network which maps the feature of $A \in \mathbf{R}^{c\times m\times n}$ to the target matrices $\gamma_\psi \in \mathbf{R}^{m\times n}$, then when the number of convolutional filter approaches to infinity, the CNTK is stated by:

$$K(X_{i,j}, X_{i',j'}) = [\Theta^L(A, A')]_{i,j,i',j'}, \tag{8}$$

where, $X_{i,j}, X_{i',j'} \in \mathbf{R}^{m,n}$ is the indicator matrices. As derived in [34], if $b(X) = X^T\gamma_\psi$ the kernel at the indicator matrices is given by:

$$\begin{aligned} K(X_{i,j}, X_{i',j'}) &= \frac{\delta_b(X_{i,j})\delta_b(X_{i',j'})}{\delta W_{i,j}\delta W_{i,j}} = \frac{\delta(\gamma_\psi(W)_{i,j})\delta(\gamma_\psi(W)_{i',j'}}{\delta W_{i,j}\delta W_{i,j}} \\ &= [\Theta^L(A, A')]_{i,j,i',j'} \end{aligned} \tag{9}$$

B. KERNEL REGRESSION WITH CNTK

The goal of kernel Regression with CNTK is to fill in unobserved entries (unobserved exposure values) as a linear combination of training examples (observed exposure values) in the sparse exposure map image.

Kernel Regression *Let $\mathcal{H}$ be a Hilbert space with inner product $\langle .,.\rangle_{\mathcal{H}}$, let $\upsilon : \mathbb{R}^d \to \mathcal{H}$ and let $K : \mathbb{R}^d \times \mathbb{R}^d \to \mathbb{R}$ be a kernel function such that $K(x, x') = \langle \upsilon(x), \upsilon(x')\rangle_{\mathcal{H}}$. Then the minimum $\mathcal{H}$-norm of the loss:*

$$\mathcal{L}(w) = \frac{1}{2}\sum_{i=1}^{n}(y^i - \langle w, \upsilon(x^i)\rangle_{\mathcal{H}})^2 \tag{10}$$

by $w = \sum_{i=1}^{n} yK_i^{-1}\upsilon(x^i$ where $K \in \mathbb{R}^{m\times n}$ is a positive definite matrix with entries $K_{i,j} = K(x_i, x_j)$. Hence the predictor is given by:

$$f(x) = yK^{-1}K'(x_i, x_j), \tag{11}$$

where, $K(x_i, x_j) \in \mathbb{R}$ is the entries in the Gram matrix. More details can be found in [52].

In this case, the sparse exposure image γ has dimensions $M \times N$ (in the following sections, we will choose $M = N = 32$) and CNTK $K \in \mathbb{R}^{M\times N\times M\times N}$.

Let $\mathbf{X}'$ be the set of measured point locations and $\mathbf{y}$ the corresponding measured values; $\mathbf{X}$ is the location of an unobserved point where we try to predict the field. The predicted value $\hat{\gamma}(\mathbf{x})$ is given by:

$$\hat{\gamma}(\mathbf{x}) = K\left(\mathbf{X}, \mathbf{X}'\right)^T_{i,j,i',j'} .K\left(\mathbf{X}, \mathbf{X}\right)^{-1}_{i,j,i',j'} .y \tag{12}$$

where $K(\mathbf{x}, \mathbf{X})$ is the CNTK evaluated between the location where the prediction is to be made and the training data X and $K(\mathbf{X}, \mathbf{X})$ is the CNTK evaluated on the training data X.

C. ARTIFICIAL NEURAL NETWORK

The ANN trained in this work was proposed in [37]. We only choose the typical ANN, with MSE loss and ADAM optimizer. The model details and training parameters are given below:

D. CONDITIONAL GENERATIVE ADVERSARIAL NETWORKS

We have used a cGAN model in a regression setting to estimate EMF exposure in 3 RoIs. The generator G and discriminator D has an ANN architecture as described

TABLE 3. ANN parameters.

Parameters	Value
Optimizer	ADAM
Kernel Initializer	he normal
Non-Linearity	ReLU
1st Layer - 4th layer	50 - 20 - 20 - 1 neurons
final layer activation	linear
Loss function	MSE
Epochs	100
Training samples	Eindhoven: 488, Utrecht: 544 Zurich: 680

in [53]. The model details and training parameters are given below:

TABLE 4. cGAN parameters.

Parameters	Value
Optimizer	G : ADAM, D: SGD
Kernel Initializer	he normal
Non-Linearity	eLU
1st Layer - 4th layer	50 - 20 - 20 - 1 neurons
final layer activation	G : linear, D: sigmoid
Loss function	G: MSE, D: BCE
Epochs	500
Training samples	Eindhoven:488, Utrecht:544, Zurich:680

REFERENCES

[1] A. M. Niknejad, S. Thyagarajan, E. Alon, Y. Wang, and C. Hull, "A circuit designer's guide to 5G mm-wave," in *Proc. IEEE Custom Integr. Circuits Conf. (CICC)*, Sep. 2015, pp. 1–8.

[2] P. Ahokangas, M. Matinmikko-Blue, S. Yrjölä, and H. Hämmäinen, "Platform configurations for local and private 5G networks in complex industrial multi-stakeholder ecosystems," *Telecommun. Policy*, vol. 45, no. 5, Jun. 2021, Art. no. 102128.

[3] P. Gajšek, P. Ravazzani, J. Wiart, J. Grellier, T. Samaras, and G. Thuróczy, "Electromagnetic field exposure assessment in Europe radiofrequency fields (10 MHz–6 GHz)," *J. Exposure Sci. Environ. Epidemiol.*, vol. 25, no. 1, pp. 37–44, Jan. 2015.

[4] C. Studer, S. Medjkouh, E. Gonultas, T. Goldstein, and O. Tirkkonen, "Channel charting: Locating users within the radio environment using channel state information," *IEEE Access*, vol. 6, pp. 47682–47698, 2018.

[5] A. Alkhateeb, G. Charan, T. Osman, A. Hredzak, J. Morais, U. Demirhan, and N. Srinivas, "DeepSense 6G: A large-scale real-world multi-modal sensing and communication dataset," *IEEE Commun. Mag.*, vol. 61, no. 9, pp. 122–128, 2023, doi: 10.1109/MCOM.006.2200730.

[6] A. Bourdoux, A. Noll Barreto, B. van Liempd, C. de Lima, D. Dardari, D. Belot, E.-S. Lohan, G. Seco-Granados, H. Sarieddeen, H. Wymeersch, J. Suutala, J. Saloranta, M. Guillaud, M. Isomursu, M. Valkama, M. Reza Kahar Aziz, R. Berkvens, T. Sanguanpuak, T. Svensson, and Y. Miao, "6G white paper on localization and sensing," 2020, *arXiv:2006.01779*.

[7] J. Hoydis, F. Ait Aoudia, A. Valcarce, and H. Viswanathan, "Toward a 6G AI-native air interface," 2020, *arXiv:2012.08285*.

[8] I. C. N.-I. R. Protection, "Guidelines for limiting exposure to electromagnetic fields (100 KHz to 300 GHz)," *Health Phys.*, vol. 118, no. 5, pp. 483–524, 2020.

[9] A. Legros et al., "Synopsis of IEEE std C95.1^{TM}-2019 'IEEE standard for safety levels with respect to human exposure to electric, magnetic, and electromagnetic fields, 0 Hz to 300 GHz," *IEEE Access*, vol. 7, pp. 171346–171356, 2019, doi: 10.1109/ACCESS.2019.2954823.

[10] S. Shepherd, M. A. P. Lima, E. E. Oliveira, S. M. Sharkh, H. Aonuma, C. W. Jackson, and P. L. Newland, "Sublethal neonicotinoid exposure attenuates the effects of electromagnetic fields on honey bee flight and learning," *Environ. Adv.*, vol. 4, Jul. 2021, Art. no. 100051.

[11] E. Egea-Lopez, F. Losilla, J. Pascual-Garcia, and J. M. Molina-Garcia-Pardo, "Vehicular networks simulation with realistic physics," *IEEE Access*, vol. 7, pp. 44021–44036, 2019.

[12] A. Forsk, "Atoll 3.4.0: User manual for radio networks," 2019.

[13] M. M. Taygur and T. F. Eibert, "A ray-tracing algorithm based on the computation of (exact) ray paths with bidirectional ray-tracing," *IEEE Trans. Antennas Propag.*, vol. 68, no. 8, pp. 6277–6286, Aug. 2020.

[14] *MATLAB Version 9.10.0.1613233 (R2021a)*, Mathworks, Inc., Natick, MA, USA, 2021.

[15] E. Basar and I. Yildirim, "SimRIS channel simulator for reconfigurable intelligent surface-empowered communication systems," in *Proc. IEEE Latin-Amer. Conf. Commun. (LATINCOM)*, Nov. 2020, pp. 1–6.

[16] S. Ju, O. Kanhere, Y. Xing, and T. S. Rappaport, "A millimeter-wave channel simulator NYUSIM with spatial consistency and human blockage," in *Proc. IEEE Global Commun. Conf. (GLOBECOM)*, Dec. 2019, pp. 1–6.

[17] M. Mallik, A. A. Tesfay, B. Allaert, R. Kassi, E. Egea-Lopez, J.-M. Molina-Garcia-Pardo, J. Wiart, D. P. Gaillot, and L. Clavier, "Towards outdoor electromagnetic field exposure mapping generation using conditional GANs," *Sensors*, vol. 22, no. 24, p. 9643, Dec. 2022.

[18] C. E. O'Lone, H. S. Dhillon, and R. M. Buehrer, "A statistical characterization of localization performance in wireless networks," *IEEE Trans. Wireless Commun.*, vol. 17, no. 9, pp. 5841–5856, Sep. 2018.

[19] R. Mathar and J. Mattfeldt, "On the distribution of cumulated interference power in Rayleigh fading channels," *Wireless Netw.*, vol. 1, no. 1, pp. 31–36, Mar. 1995.

[20] Q. Gontier, L. Petrillo, F. Rottenberg, F. Horlin, J. Wiart, C. Oestges, and P. De Doncker, "Semi-empirical model of global exposure using stochastic geometry," in *Proc. IEEE Int. Conf. Commun. Workshops (ICC Workshops)*, Jun. 2021, pp. 1–5.

[21] J. G. Andrews, F. Baccelli, and R. K. Ganti, "A tractable approach to coverage and rate in cellular networks," *IEEE Trans. Commun.*, vol. 59, no. 11, pp. 3122–3134, Nov. 2011.

[22] H. ElSawy, E. Hossain, and M. Haenggi, "Stochastic geometry for modeling, analysis, and design of multi-tier and cognitive cellular wireless networks: A survey," *IEEE Commun. Surveys Tuts.*, vol. 15, no. 3, pp. 996–1019, 3rd Quart., 2013.

[23] M. Haenggi and R. K. Ganti, "Interference in large wireless networks," *Found. Trends Netw.*, vol. 3, no. 2, pp. 127–248, 2009.

[24] H. ElSawy, E. Hossain, and M.-S. Alouini, "Analytical modeling of mode selection and power control for underlay D2D communication in cellular networks," *IEEE Trans. Commun.*, vol. 62, no. 11, pp. 4147–4161, Nov. 2014.

[25] A. M. Hayajneh, S. A. R. Zaidi, D. McLernon, and M. Ghogho, "Performance analysis of UAV enabled disaster recovery network: A stochastic geometric framework based on matern cluster processes," in *Proc. IET 3rd Int. Conf. Intell. Signal Process.(ISP)*, London, U.K., 2017, pp. 1–6, doi: 10.1049/cp.2017.0347.

[26] F. Baccelli and X. Zhang, "A correlated shadowing model for urban wireless networks," in *Proc. IEEE Conf. Comput. Commun. (INFOCOM)*, Apr. 2015, pp. 801–809.

[27] R. W. Heath, M. Kountouris, and T. Bai, "Modeling heterogeneous network interference using Poisson point processes," *IEEE Trans. Signal Process.*, vol. 61, no. 16, pp. 4114–4126, Aug. 2013.

[28] C. K. I. Williams, "Computation with infinite neural networks," *Neural Comput.*, vol. 10, no. 5, pp. 1203–1216, Jul. 1998.

[29] C. K. I. Williams, "Computing with infinite networks," in *Proc. Adv. Neural Inf. Process. Syst.*, vol. 9, Dec. 1996, pp. 295–301.

[30] J. Lee, Y. Bahri, R. Novak, S. S. Schoenholz, J. Pennington, and J. Sohl-Dickstein, "Deep neural networks as Gaussian processes," 2017, *arXiv:1711.00165*.

[31] R. Novak, L. Xiao, J. Hron, J. Lee, A. A. Alemi, J. Sohl-Dickstein, and S. S. Schoenholz, "Neural tangents: Fast and easy infinite neural networks in Python," 2019, *arXiv:1912.02803*.

[32] G. Pleiss and J. P. Cunningham, "The limitations of large width in neural networks: A deep Gaussian process perspective," 2021, *arXiv:2106.06529*.
[33] R. Novak, J. Sohl-Dickstein, and S. S. Schoenholz, "Fast finite width neural tangent kernel," in *Proc. Int. Conf. Mach. Learn.*, Jan. 2022, pp. 1–11.
[34] S. Arora, S. S. Du, W. Hu, Z. Li, R. Salakhutdinov, and R. Wang, "On exact computation with an infinitely wide neural net," in *Proc. Adv. Neural Inf. Process. Syst.*, vol. 32, Apr. 2019, pp. 8139–8148.
[35] L. Chu, H. Pan, and W. Wang, "Unsupervised shape completion via deep prior in the neural tangent kernel perspective," *ACM Trans. Graph.*, vol. 40, no. 3, pp. 1–17, Jul. 2021.
[36] A. Radhakrishnan, G. Stefanakis, M. Belkin, and C. Uhler, "Simple, fast, and flexible framework for matrix completion with infinite width neural networks," 2021, *arXiv:2108.00131*.
[37] S. Wang and J. Wiart, "Sensor-aided EMF exposure assessments in an urban environment using artificial neural networks," *Int. J. Environ. Res. Public Health*, vol. 17, no. 9, p. 3052, Apr. 2020.
[38] A. Jacot, F. Gabriel, and C. Hongler, "Neural tangent kernel: Convergence and generalization in neural networks," in *Proc. Adv. Neural Inf. Process. Syst.*, vol. 31, 2018, pp. 1–7.
[39] M. Mallik, D. P. Gaillot, and L. Clavier, "GLIP: Electromagnetic field exposure map completion by deep generative networks," 2024, *arXiv:2405.03384*.
[40] F. P. Casale, A. V. Dalca, L. Saglietti, J. Listgarten, and N. Fusi, "Gaussian process prior variational autoencoders," in *Proc. Adv. Neural Inf. Process. Syst.*, vol. 31, Jan. 2018, pp. 10369–10380.
[41] X. Pan, X. Zhan, B. Dai, D. Lin, C. C. Loy, and P. Luo, "Exploiting deep generative prior for versatile image restoration and manipulation," *IEEE Trans. Pattern Anal. Mach. Intell.*, vol. 44, no. 11, pp. 7474–7489, Nov. 2022.
[42] D. Yang and J. Sun, "Proximal dehaze-net: A prior learning-based deep network for single image dehazing," in *Proc. Eur. Conf. Comput. Vis. (ECCV)*, Jan. 2018, pp. 702–717.
[43] V. Lempitsky, A. Vedaldi, and D. Ulyanov, "Deep image prior," in *Proc. IEEE/CVF Conf. Comput. Vis. Pattern Recognit.*, Jun. 2018, pp. 9446–9454.
[44] C. Yang, X. Lu, Z. Lin, E. Shechtman, O. Wang, and H. Li, "High-resolution image inpainting using multi-scale neural patch synthesis," in *Proc. IEEE Conf. Comput. Vis. Pattern Recognit. (CVPR)*, Jul. 2017, pp. 4076–4084.
[45] M. Abadi et al., "TensorFlow: Large-scale machine learning on heterogeneous distributed systems," 2016, *arXiv:1603.04467*.
[46] P. Virtanen et al., "SciPy 1.0: Fundamental algorithms for scientific computing in Python," *Nature Methods*, vol. 17, no. 3, pp. 261–272, Feb. 2020.
[47] T. O. Hodson, "Root-mean-square error (RMSE) or mean absolute error (MAE): When to use them or not," *Geosci. Model Develop.*, vol. 15, no. 14, pp. 5481–5487, Jul. 2022.
[48] M. Deruyck, E. Tanghe, D. Plets, L. Martens, and W. Joseph, "Optimizing LTE wireless access networks towards power consumption and electromagnetic exposure of human beings," *Comput. Netw.*, vol. 94, pp. 29–40, Jan. 2016.
[49] G. Castellanos, S. De Gheselle, L. Martens, N. Kuster, W. Joseph, M. Deruyck, and S. Kuehn, "Multi-objective optimisation of human exposure for various 5G network topologies in Switzerland," *Comput. Netw.*, vol. 216, Oct. 2022, Art. no. 109255.
[50] M. Deruyck, W. Joseph, E. Tanghe, and L. Martens, "Reducing the power consumption in LTE-advanced wireless access networks by a capacity based deployment tool," *Radio Sci.*, vol. 49, no. 9, pp. 777–787, Sep. 2014.
[51] M. Mirza and S. Osindero, "Conditional generative adversarial nets," 2014, *arXiv:1411.1784*.
[52] B. Scholkopf and A. J. Smola, *Learning With Kernels: Support Vector Machines, Regularization, Optimization, and Beyond*. Cambridge, MA, USA: MIT Press, 2018.
[53] M. De Beule, E. Maes, O. De Winter, W. Vanlaere, and R. Van Impe, "Artificial neural networks and risk stratification: A promising combination," *Math. Comput. Model.*, vol. 46, nos. 1–2, pp. 88–94, Jul. 2007.

MOHAMMED MALLIK (Member, IEEE) received the master's degree in electronics and information technology in Germany and the Ph.D. degree from the University of Lille. Currently, he is with the RHODES Group, INSA Lyon, a leading French public institute of technology. His research interests include EMF exposure assessment, machine learning, and optimization.

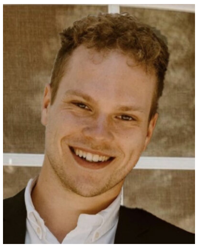

JORN SCHAMPHELEER received the M.Sc. degree in industrial engineering from Ghent Univesity, Ghent, Belgium, in 2023. He is currently pursuing the Ph.D. degree with the WAVES Research Group, Department of Information Technology, Ghent University (UGent-INTEC). Since July 2023, he has been a Research Assistant with the WAVES Research Group, UGent-INTEC. His scientific work is focused on network planning, more specifically on machine learning for network planning in mobile communication networks.

LAURENT CLAVIER (Senior Member, IEEE) received the Ph.D. degree in signal processing from TELECOM Bretagne (now IMT Atlantique), Brest, France, and the H.D.R. degree from Lille University, France, in 2009. Since October 2011, he has been a Professor with the Mines-Telecom Institute, IMT Nord Europe. He has participated in several European and French-funded projects and has published more than 150 articles and communications. His research interests include digital communications and the physical layer of wireless networks for the IoT, more specifically energy autonomous sensor networks, interference models, and impact in ultra-dense wireless networks. He is the Chair of the CA20120 "Intelligence-Enabling Radio Communications for Seamless Inclusive Interactions" (INTERACT).

MARGOT DERUYCK (Member, IEEE) was born in Kortrijk, Belgium, in July 1985. She received the M.Sc. degree in computer science engineering and the Ph.D. degree from Ghent University, Ghent, Belgium, in 2009 and 2015, respectively. From September 2009 to January 2015, she was a Research Assistant with the WAVES Research Group, Department of Information Technology, Ghent University (iMinds/UGent-INTEC). Her scientific work is focused on green wireless access networks with minimal power consumption and minimal exposure to human beings. This work led to the Ph.D. degree. Since January 2015, she has been a Postdoctoral Researcher at Ghent University and research group, where she continues her work in green wireless network planning. She is currently a Professor with Ghent University. She is also a Postdoctoral Fellow of the Research Foundation Flanders (FWO-V).